Available online at www.sciencedirect.com
ScienceDirect
International Journal of Heat and Mass Transfer 51 (2008) 3630–3641
International Journal of HEAT and MASS TRANSFER
www.elsevier.com/locate/ijhmt

Analyses of gas flows in micro- and nanochannels

Moran Wang [a,b], Xudong Lan [b], Zhixin Li [b,*]

[a] Nanomaterials in the Environment, Agriculture and Technology (NEAT), University of California, Davis, CA 95616, USA
[b] Department of Engineering Mechanics, Tsinghua University, Beijing 100084, China

Received 26 April 2006; received in revised form 10 October 2007
Available online 20 February 2008

Abstract

Micro- and nanoscale gas flows are analyzed theoretically and numerically. The analyses of gas flow similarity show that the gas flows at different scales can be similar only when the gas is treated as a prefect gas. If the gas density is so high that the density effect cannot be ignored, the three dimensionless parameters, *Re*, *Ma*, and *Kn*, which characterize the micro gas flow, are independent of each other and cannot be equal for flows at different scales, so the similarity breaks down. The critical density for the similarity failure can be analytically determined for each kind of gas. The analytical results were validated by numerical simulations. High density, high Knudsen number gas flows were modeled using a generalized Monte Carlo method based on the Enskog theory which considers both the density effect on the collision rate and the molecular repulsive and attractive interactions for a Lennard–Jones gas. The predicted transport coefficients agree better with experimental data than previous predictions. The simulation results show that when the gas density is higher than the critical density, the denseness effect alters the flow velocity and temperature fields from the direct simulation Monte Carlo results. Higher densities lead to greater deviation.

Keywords: Micro gas flow; Denseness effect; Similarity; DSMC; Lennard–Jones fluid

1. Introduction

The development of high-speed flight at high altitudes has created renewed interest in rarefied gas flows. Rarefied gas flows differ from classical gas dynamics in that the continuum hypothesis is no longer valid; therefore, the continuum hypothesis cannot be used to analyze rarefied gas flows. Rarefied gas flows are characterized by the Knudsen number, which is defined as the ratio of the molecular mean free path to a characteristic geometric length or a length over which very large variations of a macroscopic quantity may take place,

$$Kn = \frac{\lambda}{l}, \tag{1.1}$$

where λ is the molecular mean free path and l is the characteristic length. Flow regimes are classified based on the Knudsen number as [1]

- continuum flow ($Kn \leqslant 0.001$),
- slip flow ($0.001 < Kn < 0.1$),
- transition flow ($0.1 < Kn < 10$),
- free molecular flow ($Kn \geqslant 10$).

In recent years, Micro/Nano-Electro-Mechanical Systems (MEMS/NEMS) have been rapidly developed for important applications in navigation, spaceflight and industry [2]. Microscale flow systems have been developed as an important part of MEMS/NEMS [3,4]. The characteristics of these microscale flows differ greatly from those of macroscale flows. For example, at normal temperatures and pressures, velocity slip and temperature jumps, which are called rarefied gas effects, occur on the wall surfaces in microchannels [1]. Rarefied gas flows and microscale gas flows also exhibit many other similar phenomena. Previous works have shown that traditional simulation and analysis methods used for rarefied gas flows are effective for analyzing most microscale gas flows [5]. Various studies have analyzed the similarities between microscale gas flows

* Corresponding author.
E-mail address: lizhx@tsinghua.edu.cn (Z. Li).

0017-9310/$ - see front matter © 2007 Elsevier Ltd. All rights reserved.
doi:10.1016/j.ijheatmasstransfer.2007.10.011

Nomenclature

a	local sound speed (m/s)
a_v	attraction strength in van der Waals equation (J^2/mol^2 Pa)
D	self-diffusion coefficient (m^2/s)
E_t	relative translational energy (J)
k	Boltzmann constant (J/K)
Kn	Knudsen number
l	characteristic length (m)
m	molecular mass (kg)
m_r	reduced molecular mass (kg)
Ma	Mach number
n	number density (m^{-3})
p	pressure (Pa)
r	intermolecular separation (m)
R	universal gas constant (J/mol K)
Re	Reynolds number
T	gas temperature (K)
T^*	dimensionless temperature: kT/ε
U	local mean velocity (m/s)
$\bar{v}_m$	mean molecular speed (m/s)

Greek symbols

α^*	scattering coefficient for a soft-sphere model
α_j	model parameters
χ	correction factor for enhanced collisions
η	molecular volume ratio defined as $2\pi n\sigma^3/3$
γ	specific heat ratio
ζ	number of rotational degrees of freedom
λ	molecular mean free path (m)
μ	dynamic viscosity (kg/m s)
ν	kinetic viscosity (Pa s)
ρ	density (kg/m^3)
σ	molecular diameter (m)
σ_T	total collision cross-section (m^2)
ε	molecular potential well depth (J)
ε_{rot}	molecular rotational energy (J)
$\Omega^{(1,1)}$, $\Omega^{(2,2)}$	integrals for calculating the transport coefficients
$\Gamma(\ldots)$	gamma function
Γ_B	scattering probability based on Boltzmann theory
Γ'	enhanced scattering probability in a dense gas

Subscripts

c	critical state
1	case 1
2	case 2

and macroscale rarefied gas flows [1,5–7]. Gad-el-Hak [1] also used this similarity to analyze many microchannel flows.

Although the Knudsen number of a micro gas flow may be of the same magnitude as that of a rarefied gas flow, they actually come from different phenomena. In microchannel, large Knudsen numbers are caused by the small characteristic length, while in rarefied gas flows, the large Knudsen number is due to the large molecular mean free path. Therefore, they result from different mechanisms despite their similar phenomena. Wang and Li [8] reported that similarity holds only if the gas can be treated as an ideal gas. They then studied the fluid characteristics of high Knudsen number, high density gas flow in micro- and nanochannels with a consistent Boltzmann algorithm (CBA) [9,10] and the Enskog simulation Monte Carlo (ESMC) method [11]. These numerical results showed that similarity broke down at high gas densities. However, neither the CBA nor ESMC methods are completely accurate for these flows. The CBA method changes the gas transport coefficients from real values at high densities. The ESMC method is hardly able to simulate the van der Waals force effects on the flows. Thus, a new efficient numerical method for the high Knudsen number, high density gas flows is urgently necessary.

This paper provides systematic analyses and simulations of gas flows in micro- and nanoscale channels. The analyses provide the conditions when micro/nano gas flows are similar with rarefied gas flows. Then a Monte Carlo method is used to provide correct predictions of high Knudsen number, high density gas flows. The characteristics of such flows are then investigated based on the results.

2. Theoretical analysis

2.1. Similarity of perfect gas

Both micro gas flows and rarefied gas flows have three dimensionless numbers that characterize the flows: the Reynolds number, Re, the Mach number, Ma, and the Knudsen number, Kn. However, these three parameters are not independent in rarefied gas flows but are related by [7],

$$Kn = \sqrt{\frac{\pi\gamma}{2}}\frac{Ma}{Re}. \tag{2.1}$$

Several researchers have used this relationship for rarefied gas flows in microscale gas flow analyses [1,5,6]. However, this relationship has limited applications in micro gas flows. Wang and Li [8] applied this relationship to microscale flows to show that Eq. (2.1) is based on a relationship between the viscosity and the mean free path. With gas kinetic theory, when the gas molecules are treated as

smooth rigid sphere with only a repelling force, the kinetic viscosity can be simply related to the molecular mean free path as

$$v = \frac{1}{2}\lambda \bar{v}_{\mathrm{m}}, \tag{2.2}$$

where $\bar{v}_{\mathrm{m}}$ is the molecular mean speed which is somewhat higher than the sound speed a:

$$\bar{v}_{\mathrm{m}} = \sqrt{\frac{8}{\pi\gamma}}a. \tag{2.3}$$

With this assumption for Eq. (2.2), if the gas is a perfect gas, the three dimensionless numbers are not independent. As a result, gas flows at different scales can be similar (if other similarity conditions are also satisfied such as similar geometries and boundary conditions). Therefore, for such conditions, micro gas flows can be assumed to be similar to rarefied gas flows. Since rarefied gas flows have been studied extensively due to their important applications in astronautics and aeronautics, many theories and much experimental data can be used for micro gas flow analysis by the similarity [8].

2.2. Similarity failure in dense gas flows

However, the perfect gas assumption does not always hold in micro gas flows. When the gas density is high or the temperature is low, intermolecular attractions become significant as the denseness effect changes the gas flow characteristics. According to Enskog's theory, the gas molecular mean free path in a dense gas, λ, is given by [12]:

$$\lambda = [\sqrt{2}\pi n\chi\sigma^2]^{-1}, \tag{2.4}$$

where χ is the enhanced collision correction factor, which is a function of the gas density, which will be determined later. The dynamic viscosity, μ', including the density effect, is related to μ for a perfect gas by

$$\mu' = \mu\cdot\eta[(\eta\chi)^{-1} + 0.8 + 0.7614(\eta\chi)], \tag{2.5}$$

where $\eta = 2\pi n\sigma^3/3$ represents the molecular volume ratio. From classical thermodynamic theory, the sound speed in a dense gas is enhanced by

$$a' = a\left[1 + 8\eta\chi + \frac{4}{5}\eta^2\left(8\chi^2 + 3\frac{\mathrm{d}\chi}{\mathrm{d}\eta}\right)\right]^{1/2}. \tag{2.6}$$

In perfect gas flow, since Kn, Ma and Re are not independent, if two of these numbers in two flows at different scales are equal, then the other one must also be equal. The two flows at different scales are then similar as a result. However, in dense gas flows this relationship does not hold.

For convenience, assume Re and Ma are equal in the two systems:

$$Re_1 = Re_2, \tag{2.7}$$

and

$$Ma_1 = Ma_2. \tag{2.8}$$

Then, from Eqs. (2.4)–(2.6),

$$\frac{U_1 l_1\rho_1}{[(\eta_1\chi_1)^{-1} + 0.8 + 0.7614\eta_1\chi_1]\eta_1} = \frac{U_2 l_2\rho_2}{[(\eta_2\chi_2)^{-1} + 0.8 + 0.7614\eta_2\chi_2]\eta_2}, \tag{2.9}$$

$$\frac{U_1}{\sqrt{T_1}\left[1 + 8\eta_1\chi_1 + \frac{4}{5}\eta_1^2\left(8\chi_1^2 + 3\frac{\mathrm{d}\chi_1}{\mathrm{d}\eta}\right)\right]^{1/2}} = \frac{U_2}{\sqrt{T_2}\left[1 + 8\eta_2\chi_2 + \frac{4}{5}\eta_2^2\left(8\chi_2^2 + 3\frac{\mathrm{d}\chi_2}{\mathrm{d}\eta}\right)\right]^{1/2}}. \tag{2.10}$$

The Knudsen numbers are

$$Kn_1 = \frac{\lambda_1}{l_1} = \frac{[\sqrt{2}\pi n_1\chi_1(\eta_1)\sigma^2]^{-1}}{l_1}, \tag{2.11}$$

$$Kn_2 = \frac{\lambda_2}{l_2} = \frac{[\sqrt{2}\pi n_2\chi_2(\eta_2)\sigma^2]^{-1}}{l_2}. \tag{2.12}$$

Dividing Eq. (2.11) by Eq. (2.12) gives

$$\frac{Kn_1}{Kn_2} = \frac{l_2\eta_2\chi_2}{l_1\eta_1\chi_1}. \tag{2.13}$$

Then from Eqs. (2.9) and (2.10):

$$\frac{l_2}{l_1} = \frac{[(\eta_2\chi_2)^{-1} + 0.8 + 0.7614\eta_2\chi_2]\eta_2\rho_1 U_1}{[(\eta_1\chi_1)^{-1} + 0.8 + 0.7614\eta_1\chi_1]\eta_1\rho_2 U_2}, \tag{2.14}$$

$$\frac{U_1}{U_2} = \frac{\sqrt{T_1}}{\sqrt{T_2}}\cdot\frac{\left[1 + 8\eta_1\chi_1 + \frac{4}{5}\eta_1^2(8\chi_1^2 + 3\chi_1')\right]^{1/2}}{\left[1 + 8\eta_2\chi_2 + \frac{4}{5}\eta_2^2(8\chi_2^2 + 3\chi_2')\right]^{1/2}}. \tag{2.15}$$

Substituting Eqs. (2.14) and (2.15) into Eq. (2.13) leads to

$$\frac{Kn_1}{Kn_2} = \frac{\sqrt{T_1}}{\sqrt{T_2}}\cdot\frac{\left[1 + 8\eta_1\chi_1 + \frac{4}{5}\eta_1^2\left(8\chi_1^2 + 3\frac{\mathrm{d}\chi_1}{\mathrm{d}\eta}\right)\right]^{1/2}}{\left[1 + 8\eta_2\chi_2 + \frac{4}{5}\eta_2^2\left(8\chi_2^2 + 3\frac{\mathrm{d}\chi_2}{\mathrm{d}\eta}\right)\right]^{1/2}} \cdot\frac{[1 + 0.8\eta_2\chi_2 + 0.7614(\eta_2\chi_2)^2]}{[1 + 0.8\eta_1\chi_1 + 0.7614(\eta_1\chi_1)^2]}. \tag{2.16}$$

If the dense gas flows at different scales are similar, Kn_1 should be equal to Kn_2. Therefore the right hand side of Eq. (2.16) must be equal to unity. Because of the nonlinear nature of the right hand side of Eq. (2.16), the equation was evaluated numerically for various conditions at $T_1 = T_2$.

The numerator and denominator of the right hand side of Eq. (2.16) are functions of the gas number density:

$$f_1 = \left[1 + 8\eta_1\chi_1 + \frac{4}{5}\eta_1^2\left(8\chi_1^2 + 3\frac{\mathrm{d}\chi_1}{\mathrm{d}\eta}\right)\right]^{1/2} \times [1 + 0.8\eta_2\chi_2 + 0.7614(\eta_2\chi_2)^2], \tag{2.17}$$

$$f_2 = \left[1 + 8\eta_2\chi_2 + \frac{4}{5}\eta_2^2\left(8\chi_2^2 + 3\frac{\mathrm{d}\chi_2}{\mathrm{d}\eta}\right)\right]^{1/2} \times [1 + 0.8\eta_1\chi_1 + 0.7614(\eta_1\chi_1)^2], \tag{2.18}$$

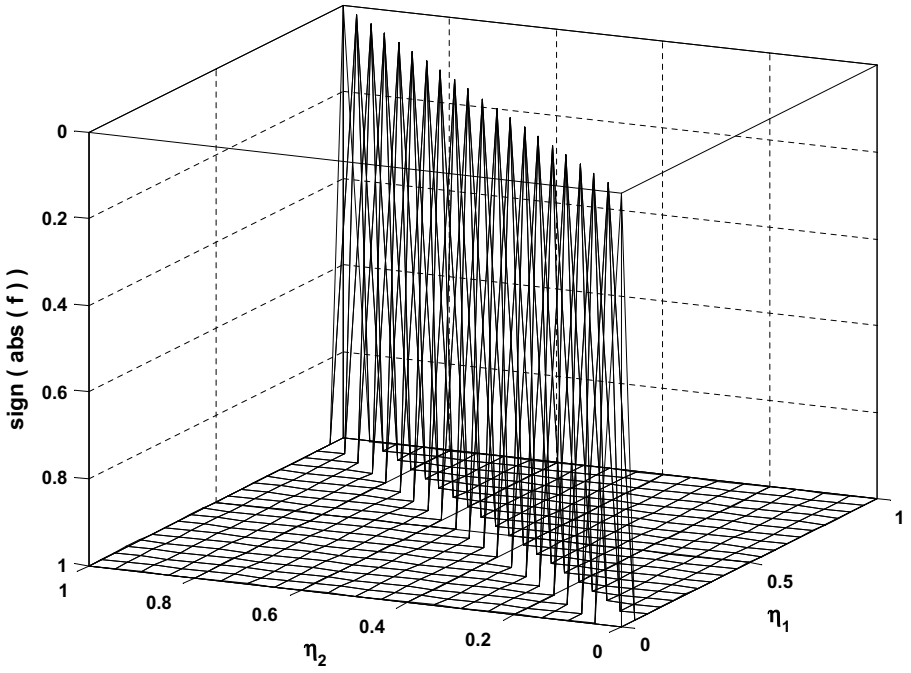

Fig. 1. Variation of the Knudsen number ratio for dense gases as represented by f as functions of the molecular densities of the two gases, η_1 and η_2.

where $\eta_1,\eta_2 \in [0,1)$. Defining f as the difference between f_1 and f_2, if f is equal to zero, then $f_1 = f_2$ and, therefore, $Kn_1 = Kn_2$. Fig. 1 shows the sign function of the absolute value of f for various values of η_1 and η_2 which are proportional to the gas densities. The result indicates that $f_1 = f_2$ ($Kn_1 = Kn_2$) only when $\eta_1 = \eta_2$. A detailed data analysis also validated this result. Thus, the characteristic lengths must be the same if the two dense gas flows are similar. If $\eta_1 \neq \eta_2$ (namely $l_1 \neq l_2$), $Kn_1 \neq Kn_2$. Therefore, the three dimensionless parameters in dense gas flows at different scales cannot be equal, and the two flows cannot be similar.

The high gas density affects the gas characteristics such as the viscosity and the sound speed which then affect the dimensionless parameters. Therefore, a critical density can be specified so that for densities below this critical density, the perfect gas assumption and the similarity between gas flows holds. The critical density can be calculated based on Eqs. (2.4)–(2.6) for a specified deviation of 5%. For nitrogen gas as an example, the critical density for the perfect gas assumption is

$$\rho_c \approx 4.5\rho_0, \tag{2.19}$$

where ρ_0 is the density at standard state using the gas parameters in Hirschfelder et al. [13]. Eq. (2.19) indicates the denseness effect must be considered when the micro-scale flow density is larger than 4.5 times the standard state density. Critical values for several often gases are listed in Table 1. The results show that larger molecular diameter leads to a smaller critical density with (SO_2) having a critical density less than three times the standard state density, while the value for (He) is larger than 13 times the standard state density.

Table 1
Critical densities for various gases

Gas type	ρ_c/ρ_0	Gas type	ρ_c/ρ_0
SO_2	2.72	NO	5.33
CO_2	3.49	NH_3	5.47
CH_4	3.81	O_2	5.51
N_2O	3.82	Ar	5.58
N_2	4.47	H_2	8.53
Air	4.71	Ne	10.27
CO	4.82	He	13.04

The molecular parameters were taken from Hirschfelder et al. (1954 Table. 8.4-1).

3. Numerical simulations

Numerical simulations were performed to validate the theoretical analyses. A hard sphere model of the direct simulation Monte Carlo (DSMC) method was used to verify the similarity of gas flows that are perfect gases. For the high density, high Knudsen number gas flows, we used a new Monte Carlo method, generalized Enskog Monte Carlo (GEMC), to simulate the dense gas flows in micro- and nanochannels.

3.1. Direct simulation Monte Carlo method

The DSMC method is a molecular-based statistical simulation method for rarefied gas flows introduced by Bird [14]. The method numerically solves the dynamic equations for the gas flow using thousands of simulated molecules. Each simulated molecule represents a large number of real molecules. Assuming molecular chaos and a rarefied gas, only binary collisions need be considered, so the molecular

motion and the collisions are uncoupled if the computational time step is smaller than the physical collision time. Interactions with boundaries and with other molecules conserve both momentum and energy. The macroscopic flow characteristics are obtained by statistically sampling the molecular properties in each cell. At the beginning of the calculation, the simulated particles are uniformly distributed in the cells. In each time step, all particles move according to their individual velocities, interact with the boundaries and are then indexed. A number of collision pairs are selected in each cell using the no-time-counter (NTC) method for the collision calculations. These steps are repeated with increased sample sizes until the statistical errors are small. The DSMC method can simulate non-equilibrium and unsteady gas flows. A steady-state flow field is obtained with a sufficiently long simulation time.

The variable hard sphere (VHS) model [14] incorporates the hard sphere scattering law for collisions and treats the molecular cross-sections as functions of the relative translational energy during the collision. In the VHS model, the gas molecules are actually treated as hard spheres with only a repelling force, which is consistent with the perfect gas assumption. The time step used in DSMC method should be less than the mean collision time and the cell (or subcell) size should be less than the mean free path in the simulated situation. Violation of this condition may produce solutions that are not physically realistic [15–17].

The wall temperature was all assumed to be equal. When the simulated particle collides with the wall, the diffuse reflection model is used to determine the reflection. In this model, the emission of molecules impinging on the wall is not correlated with the pre-impingement state of the molecules. The outgoing velocity is randomly assigned according to a half-range Maxwellian distribution determined by the wall temperature. This is also known as the full thermal and momentum accommodation method [18,19]. We use freestream boundary conditions at both inlet and outlet of a channel [14,20].

3.2. Generalized Enskog Monte Carlo method

Dense gas flows have two distinctive characteristics that require a different type of analysis from rarefied gas flows: the collisions are much more frequent and the van der Waals force cannot be ignored. Alexander et al. [21] developed a consistent Boltzmann algorithm (CBA) to expand the DSMC method to dense gases and even liquids by introducing an additional displacement after the molecular collisions. This modification adapts the gas properties described by the van der Waals equation instead of by the equation of state (EOS) for a perfect gas. This method has been applied to model gas–liquid interface characteristics [22], and micro and nanoscale non-ideal gas flows [9,10]. However, the additional displacement changed not only the EOS but also the gas transport characteristics. As a result, when the ratio of the gas molecular volume to the whole volume is relatively high, the gas transport characteristics become unrealistic and the predictions fail [23–25,11].

Other method was developed based on Enskog dense gas theory. Enskog developed the Enskog equation (EE) for hard spheres to incorporate finite-density effects. His two significant changes were the finite distance between the centers of a colliding pair and the increased collision frequency due to excluded volume effects [26]. Montanero et al. [27–29] then developed an Enskog simulation Monte Carlo (ESMC) method which extended Bird's DSMC for a hard sphere fluid at finite densities. However, the ESMC methods did not include attractive interactions between molecules, therefore, the transport properties predicted by the ESMC methods did not agree well with the experimental data or the theoretical values [11].

This paper uses a generalized Enskog Monte Carlo method (GEMC) developed by Wang and Li [30]. The method employs the Lennard–Jones (L–J) potential between molecules with a generalized collision model introduced into the Monte Carlo method. The method also considers the finite-density effects on the molecular collision rate and transport properties to obtain an equation of state for non-ideal gases. The resulted transport properties agree better with experimental data and theoretical values than previous methods for dense gas flow predictions. The main idea is described as follows and the details can be found in Ref. [30].

In actual gases the force between two molecules is repulsive at small distances and weakly attractive at larger distances. This behavior is most simply described by the Lennard–Jones (6–12) potential [12]

$$\varphi(r) = 4\varepsilon\left[\left(\frac{\sigma}{r}\right)^{12} - \left(\frac{\sigma}{r}\right)^{6}\right], \tag{3.1}$$

where σ denotes the low-velocity diameter and ε is the depth of the potential well, which are constants characteristic of the chemical species of the colliding molecules, and r is the intermolecular separation. This potential has been found to be adequate for a number of nonpolar molecules. Many efforts have been made to establish collision models to include the Lennard–Jones potential in the molecular interaction process [31,32]. These models have defined the total collision cross-section as

$$\frac{\sigma_T}{\sigma^2} = \sum \alpha_j \left(\frac{E_t}{\varepsilon}\right)^{-\omega_j}, \tag{3.2}$$

where σ_T is the total collision cross-section, E_t denotes the relative translational energy, the parameters ω_j are related to the Lennard–Jones potential [31], and α_j are determined from the transport property data, depending on whether the interaction is between like or unlike molecules. The coefficients of viscosity and self-diffusion of a simple gas, to the first approximation, are expressed as functions of temperature by [12]

$$\mu = \frac{5}{16}\left(\frac{(\pi mkT)^{1/2}}{\pi\sigma^2\Omega^{(2,2)^*}}\right), \tag{3.3}$$

$$D = \frac{3}{16}\left(\frac{(2\pi kT/m_r)^{1/2}}{n\pi\sigma^2\Omega^{(1,1)^*}}\right), \tag{3.4}$$

where m is the particle mass, k is the Boltzmann constant, n is the number density and $\Omega^{(1,1)^*}$ and $\Omega^{(2,2)^*}$ are integrals for calculating the transport coefficients for the Lennard–Jones potential [13]. For a L–J gas model with a total collision cross-section given by Eq. (3.1), the self-diffusion and viscosity integrals are

$$\Omega^{(1,1)^*} = \frac{1}{\pi(\alpha^*+1)}\sum \alpha_j \Gamma(3-\omega_j) T_*^{-\omega_j}, \tag{3.5}$$

$$\Omega^{(2,2)^*} = \frac{\alpha^*}{\pi(\alpha^*+1)(\alpha^*+2)}\sum \alpha_j \Gamma(4-\omega_j) T_*^{-\omega_j}, \tag{3.6}$$

where α^* denotes the scattering coefficient for a soft-sphere model, $T^* = kT/\varepsilon$, and $\Gamma(\ldots)$ denotes the gamma function. These parameters can be determined by numerical fitting using the data of $\Omega^{(2,2)^*}$ tabulated in, Table I–M of Hirschfelder et al. [13]. Such a significant job has been found in the GSS model [32,33]. We are here employing Fan's results of the parameter values: $\alpha_1 = 3.962$, $\alpha_2 = 4.558$, $\omega_1 = 0.133$,

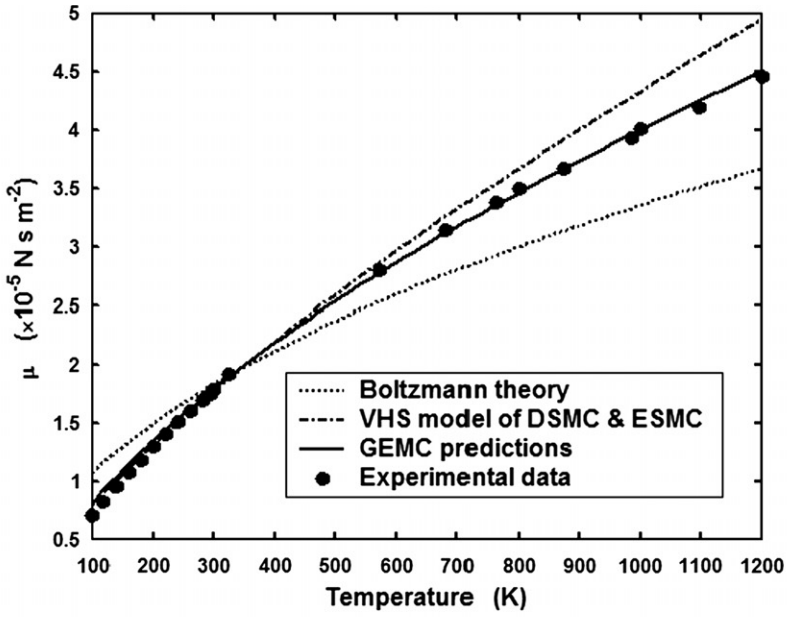

(a) viscosity versus temperature at low or moderate gas densities.

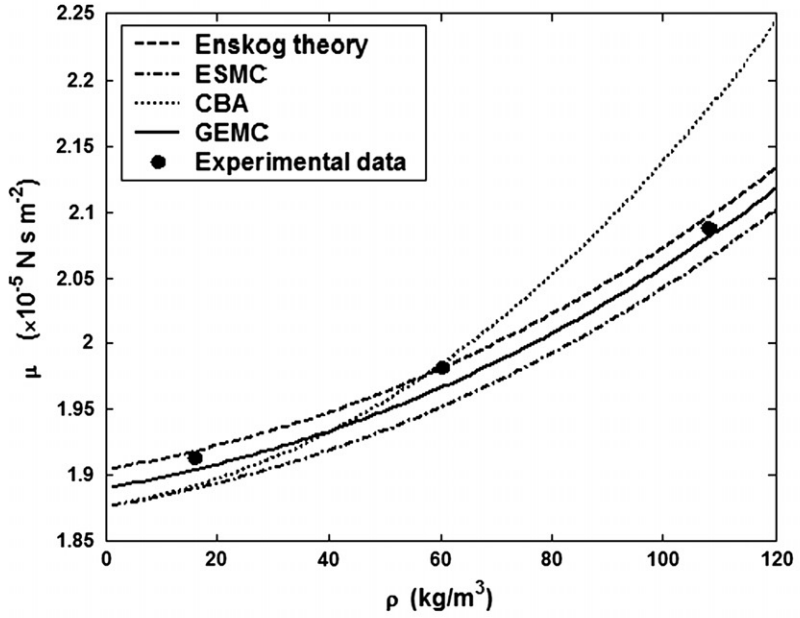

(b) viscosity versus density below 150×10^5 Pa. The CBA method uses $d_{vdW} = \sigma$.

Fig. 2. Viscosities predicted by the present method compared with experimental data and other models.

$\omega_2 = 1.25$ and $\alpha^* = 1.5$. These values are generally suitable for simple nonpolar gases.

Based on the Enskog equation for dense gases [26], when a gas is so dense that the *co*volume of the molecules is comparable with the total system volume, the molecules can no longer be treated as point particles. Therefore, the common position of two colliding molecules in the Boltzmann equation should be replaced by the actual positions of the centers of two tangent spheres. The collision frequency is influenced by *co*relational effects that depend on the density at the point of contact.

A modified higher scattering probability due to the reduced volume occupied by the molecules is

$$\Gamma' = (1 - 4n\pi\sigma^3/3)\Gamma_B. \tag{3.7}$$

However, the scattering probability is lowered again by the particles screening each other. A particle might not be available for scattering with another particle because there might be a third particle in between. This effect leads to a reduction of the scattering probability by a factor $(1 - 11n\pi\sigma^3/12)$. With this factor, the modified scattering probability is

$$\Gamma' = \chi \cdot \Gamma_B, \tag{3.8}$$

where $\chi(\eta) = \frac{1-11\eta/8}{1-2\eta}$.

This result can, however, be trusted for low orders of n, since four particle configurations have not been considered. The expression up to third order is [26]

$$\chi(\eta) = 1 + 0.625\eta + 0.2869\eta^2 + 0.1103\eta^3. \tag{3.9}$$

In the standard Enskog theory, the pressure in a dense gas is

$$p = knT[1 + \eta\chi]. \tag{3.10}$$

However, Enskog preferred a different procedure based on the close relation between $(\eta \cdot \chi)$ and the compressibility. He observed that, if the hard sphere molecules are surrounded by weak attractive fields of force, the equation of state would be modified to the following form

$$p + a_v\rho^2 = knT[1 + \eta\chi], \tag{3.11}$$

where a_v denotes the strength of the attraction, which is independent of the temperature and dependent on the gas properties [34]

$$a_v = \frac{27}{64}\frac{R^2T_c^2}{p_c}, \tag{3.12}$$

where R denotes the gas constant, T_c the critical temperature, and p_c the critical pressure.

Thus GEMC method solves the Enskog equation for a dense gas statistically while keeping the gas transport properties in good agreement with experimental data. The transport coefficient viscosity from this method is compared with predictions from other methods and experimental data [13] in Fig. 2a which shows the viscosity changes with temperature at low or moderate gas densities. The GEMC method gives much better agreement with experimental data at both lower and higher temperatures than the Boltzmann theory or the viscosity–temperature power law used in the variable hard sphere (VHS) model in the DSMC or ESMC methods. The viscosity changes with density below 150×10^5 Pa pressures are shown in Fig. 2b. The GEMC predictions agrees well with the experimental data and the Enskog theory, while the CBA and DSMC methods deviate from the experimental data at high gas densities. Therefore, the GEMC method gives the best agreements with experimental data over a large of temperatures and densities.

4. Simulation results and discussion

4.1. Similarity of perfect gas flows

When a gas is treated as a perfect gas, flows at different scales will be similar. This analytical result was numerically validated by the DSMC simulations in the variable hard sphere model.

The physical model is shown in Fig. 3. The channel aspect ratio was set to 5 for all cases. The computational grid contained rectangular cells (100×60) with four subcells (2×2) per cell. The working fluid was nitrogen with the properties listed in Table 2. Table 3 lists the conditions

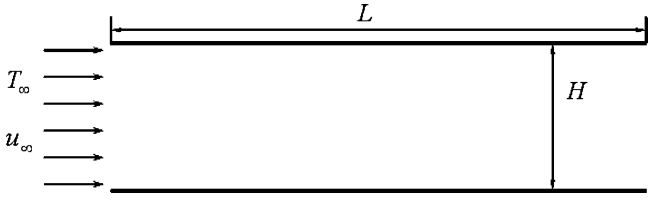

Fig. 3. Schematic of the physical problem.

Table 2
Properties of N_2

m (kg)	ζ	d_{ref} (m)	T_{ref}	ω
4.65×10^{-26}	2	4.17×10^{-10}	273	0.74

m is the gas molecular mass, ζ is the number of internal degrees of freedom, d_{ref} is the reference molecular diameter, T_{ref} is the reference temperature and ω is the viscosity temperature index.

Table 3
Simulation conditions for subsonic channel flow ($Kn = 1$, $Ma = 0.57$, $T_\infty = 300$ K, $T_w = 300$ K)

Case	H (m)	n_∞	N_{total}	N_{sample}
1	1	1.29×10^{18}	101,133	1,011,050
2	1×10^{-3}	1.29×10^{21}	101,253	1,005,050
3	1×10^{-6}	1.29×10^{24}	101,552	1,010,050
4	1×10^{-8}	1.29×10^{26}	101,329	1,010,050

H is the height of the computational domain, n_∞ is the gas molecular number density of the inlet flow, N_{total} represents the total number of simulated particles and N_{sample} is the number of time steps.

for the four subsonic channel flows. The channel height, H, was varied from one meter to ten nanometers. The freestream temperature, T_∞, as well as the temperatures of both walls, were set at 300 K. The Knudsen number and Mach number of the incoming gas flow were unity and 0.57 for all cases. Over 10^5 molecules were used in each simulation with over 10^6 times steps for each case.

The temperature and x-direction velocity profiles at the inlet and outlet are compared in Figs. 4 and 5 for the four cases. The macroscale rarefied gas flow and the microscale dense gas flow both have the same velocity slips and temperature jumps as long as the Knudsen numbers are equal. The velocity and temperature profiles were also almost the same for the different scales with the differences in the curves caused by statistical fluctuations.

4.2. Denseness effects

Table 4 lists the conditions for the three cases used to study the effect of gas density on the subsonic flow in micro- and nanochannels. The aspect ratio, L/H, was 5.0 for all three cases with uniform rectangular cells (100×60) used in the analysis. The freestream velocity, u_∞, and the temperature, T_∞, were imposed as the boundary conditions at the inlet. The temperatures of both walls were the same as the freestream gas temperature.

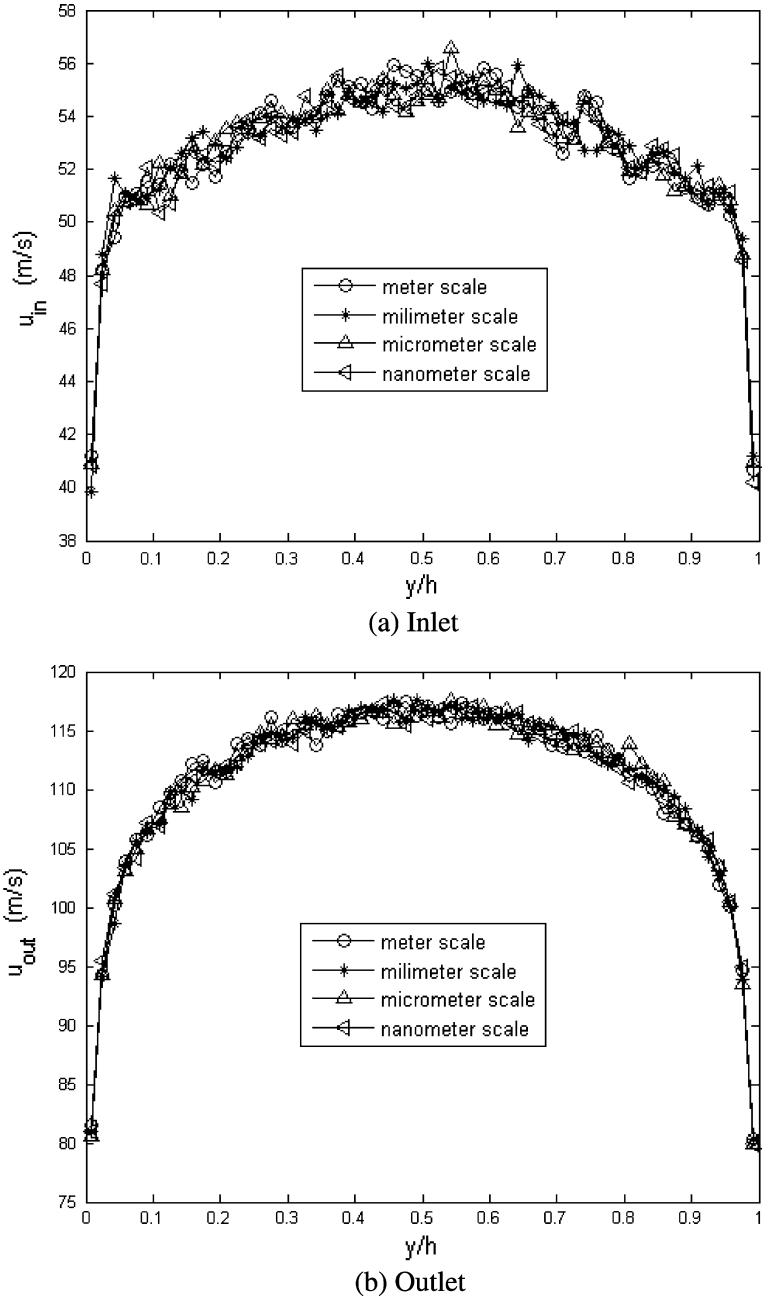

Fig. 4. Inlet and outlet x-direction velocity profiles at $Kn = 1.0$ and $Ma = 0.57$.

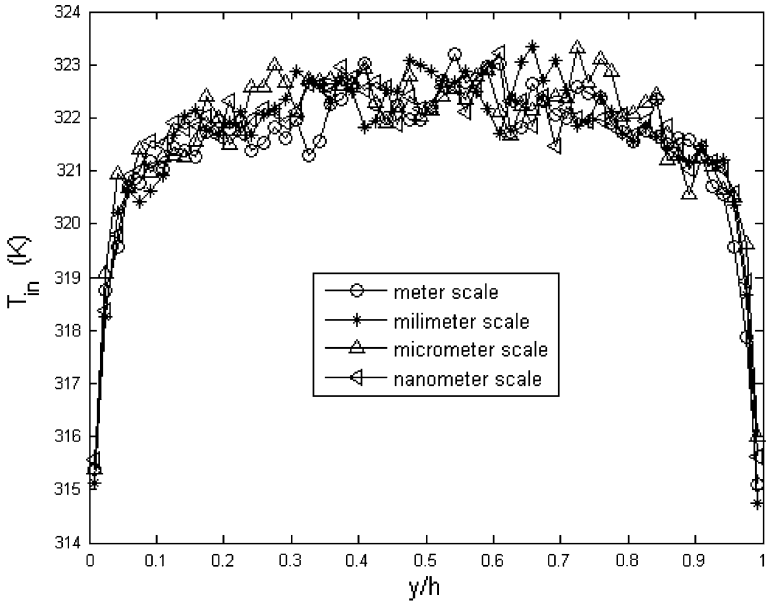

(a) Inlet

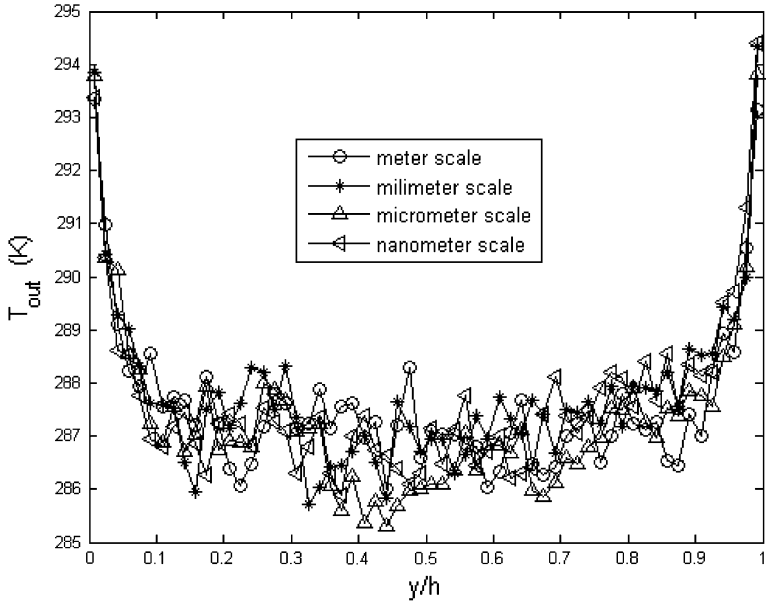

(b) Outlet

Fig. 5. Inlet and outlet temperature profiles at $Kn = 1.0$ and $Ma = 0.57$.

Table 4
Simulation conditions for density effect ($Kn = 0.05$, $u_\infty = 200$ m/s, $T_\infty = 300$ K, $T_w = 300$ K)

Cases	H (μm)	n_∞	ρ_c/ρ_0	N_{total}	N_{sample}
1	1	2.59×10^{25}	1.186	57,042	500,000
2	0.1	2.59×10^{26}	11.88	57,117	301,050
3	0.01	2.59×10^{27}	118.7	99,687	257,050

Figs. 6 and 7 show the GEMC results for the velocity and temperature profiles at the inlet and outlet for various channel sizes and $Kn = 0.05$. For comparison, the DSMC results with the perfect gas assumption are also plotted in the figures. The results show that when the gas density is not high (case 1, $\rho_c/\rho_0 = 1.186 < 4.5$), the GEMC results almost overlap the DSMC results with the fluctuations in the profiles coming from statistical variations. When the gas density is moderately high (case 2, $\rho_c/\rho_0 = 11.88 > 4.5$), the perfect gas assumption breaks down and the GEMC results begin depart from the DSMC results. As the density increases (case 3, $\rho_c/\rho_0 = 118.7$), the deviations between the GEMC results and the DSMC results increases significantly. Note that the abnormal temperature distributions near the wall surfaces predicted by the CBA method do not occur [9]. These results indicate that when the density is larger than the critical density, ρ_c, the denseness effect on the flow and heat transfer characteristics must be considered.

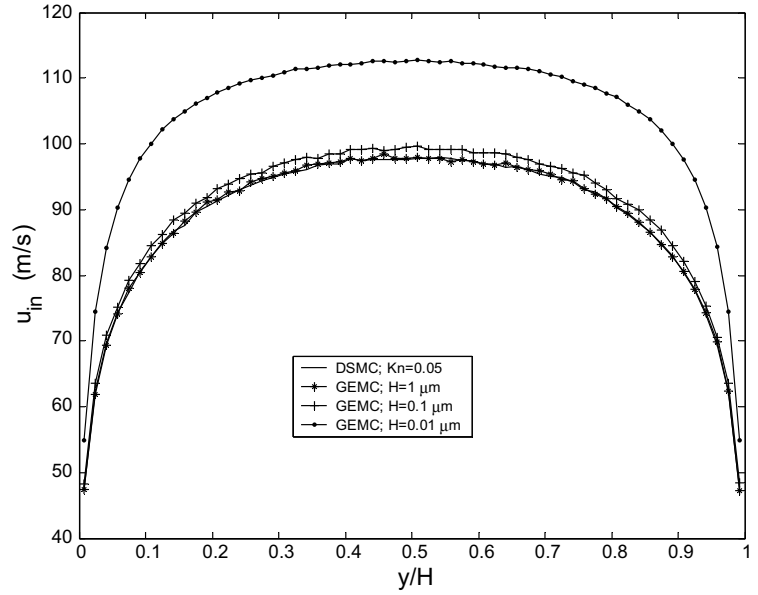

(a) Inlet

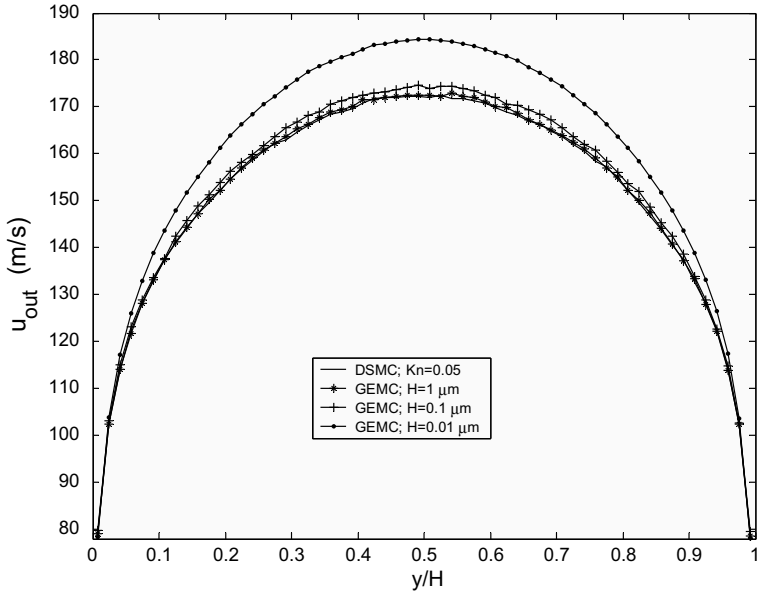

(b) Outlet

Fig. 6. Inlet and outlet velocity distributions for $Kn = 0.05$.

5. Conclusions

The theoretical and numerical analyses of micro- and nanoscale gas flows show that

(1) Microscale gas flows will be similar to normal-scale rarefied gas flows only when the gas is a perfect gas. When the gas is so dense that the density affects the gas characteristics, then the three dimensionless parameters are independent of each other, and the dimensionless parameters for the two different scale flows cannot be equal, meaning that the two flows cannot be similar.

(2) The critical densities for which similarity fails were determined analytically with different gases having different critical densities. A large molecular diameter leads to a smaller critical density. For the most commonly used gases, nitrogen and air, the critical densities are both about five times that of the standard state using the molecular parameters in Hirschfelder et al.'s book.

(3) The analytical results were validated by numerical calculations. The dense gas flow was properly simulated using a generalized Enkog Monte Carlo (GEMC) method which considers both the high density effect on the collision rate and the molecular

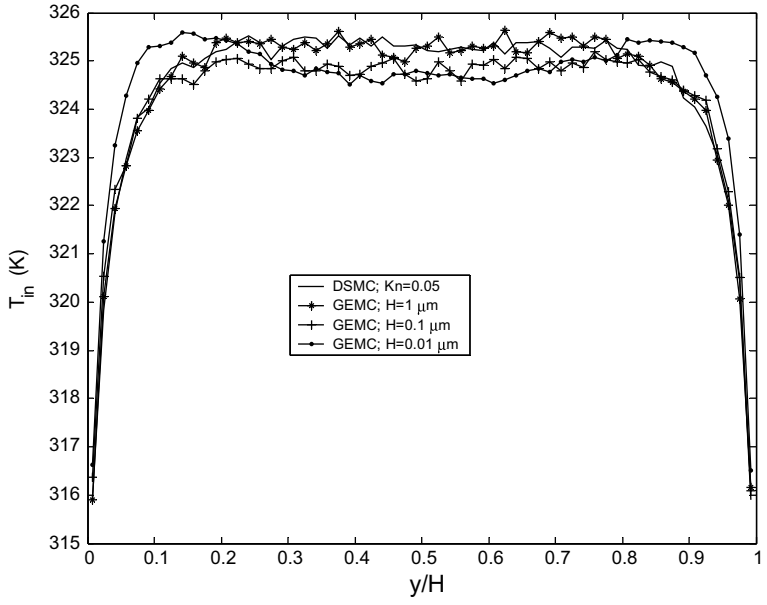

(a) Inlet

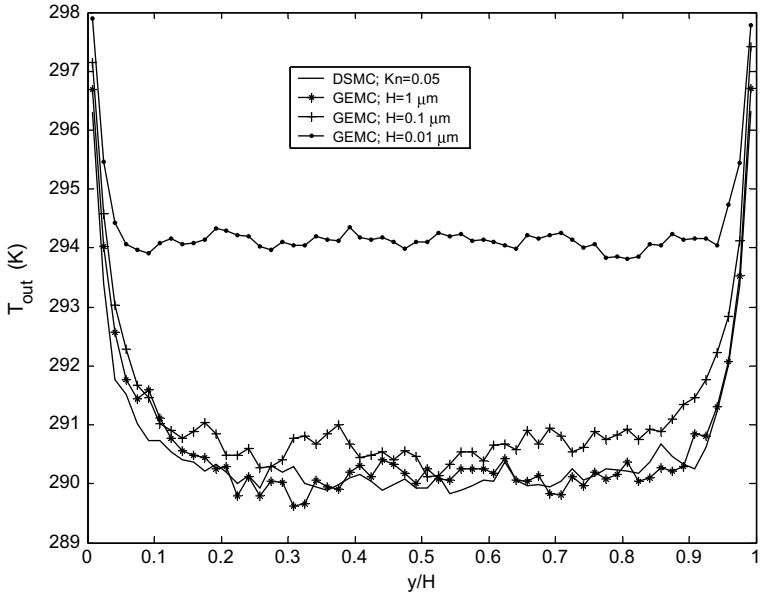

(b) Outlet

Fig. 7. Inlet and outlet temperature distributions for $Kn = 0.05$.

repulsive and attractive interactions for a Lennard–Jones fluid. The predicted transport coefficients agree better with experimental data than the previous methods. The simulation results show that when the gas density is higher than the critical density, the velocity and temperature fields differ from the predictions of the DSMC method with large differences at very high densities.

References

[1] M. Gad-el-Hak, The fluid mechanics of microdevices—the freeman scholar lecture, J. Fluid Eng. 121 (1999) 5–33.

[2] C.M. Ho, Y.C. Tai, Micro-electro-mechanical-systems (MEMS) and fluid flows, Annu. Rev. Fluid Mech. 30 (1998) 579–612.

[3] Z.Y. Guo, Z.X. Li, Size effect on microscale single-phase flow and heat transfer, Int. J. Heat Mass Transfer 46 (1) (2003) 149–159.

[4] N.T. Nguyen, S.T. Wereley, Fundamentals and Applications of Microfluidics, second ed., Artech House, 2006.

[5] G.E. Karniadakis, A. Beskok, Micro Flows: Fundamentals and Simulation, Springer, New York, 2002.

[6] F.H. Qin, D.J. Sun, X.Y. Yin, Discussion about the similarity of microscale gas flows, Int. J. Nonlinear Sci. Num. Simul. 3 (3–4) (2002) 573–576.

[7] C. Shen, Rarefied Gas Dynamics, National Defence Industry Publishing House, Beijing, 2003.

[8] M. Wang, Z.X. Li, Similarity of ideal gas flow at different scales, Sci.China Ser. E 46 (6) (2003) 621–622.

[9] M. Wang, Z.X. Li, Nonideal gas flow and heat transfer in micro- and nanochannels using the direct simulation Monte Carlo method, Phys. Rev. E 68 (2003) 046704.
[10] M. Wang, Z.X. Li, Micro- and nanoscale non-ideal gas poiseuille flows in a consistent Boltzmann algorithm model, J. Micromech. Microeng. 14 (7) (2004) 1057–1063.
[11] M. Wang, Z.X. Li, Monte Carlo simulations of dense gas flow and heat transfer in micro- and nano-channels, Sci. China Ser. E 48 (3) (2005) 317–325.
[12] S. Chapman, T.G. Cowling, The Mathematical Theory of Non-uniform Gases, Cambridge University Press, 1970.
[13] J.O. Hirschfelder, C.F. Curtiss, R.B. Bird, Molecular Theory of Gases and Liquids, Wiley, New York, 1954.
[14] G.A. Bird, Molecular Gas Dynamics and the Direct Simulation of Gas Flows, Clarendon Press, Oxford, 1994.
[15] A.L. Garcia, W. Wagner, Time step truncation error in direct simulation Monte Carlo, Phys. Fluids 12 (2000) 2621–2633.
[16] N.G. Hadjiconstantinou, Analysis of discretization in the direct simulation Monte Carlo, Phys. Fluids 12 (2000) 2634–2638.
[17] M. Wang, Z.X. Li, Gas mixing in microchannels using the direct simulation Monte Carlo method, Int. J. Heat Mass Transfer 49 (2006) 1696–1702.
[18] W.W. Liou, Y.C. Fang, Heat transfer in microchannel devices using DSMC, J. Microelectromech. Syst. 10 (2001) 274–279.
[19] M.R. Wang, Z.X. Li, Simulations for gas flows in microgeometries using the direct simulation Monte Carlo method, Int. J. Heat Fluid Flow 25 (6) (2004) 975–985.
[20] X. Wang, Q.W. Wang, W.Q. Tao, P. Zheng, Simulation of rarefied gas flow and heat transfer in microchannels, Sci. China Ser. E 45 (3) (2002) 321–327.
[21] F.J. Alexander, A.L. Garcia, B.J. Alder, A consistent Boltzmann algorithm, Phys. Rev. Lett. 74 (1995) 5212–5215.
[22] N.G. Hadjiconstantinou, A.L. Garcia, B.J. Alder, The surface properties of a van der Waals fluid, Physica A 281 (2000) 337–347.
[23] F.J. Alexander, A.L. Garcia, B.J. Alder, The consistent Boltzmann algorithm for the van der Waals equation of state, Physica A 240 (1997) 196–201.
[24] A.L. Garcia, F.J. Alexander, B.J. Alder, A particle method with adjustable transport properties—the generalized consistent Boltzmann algorithm, J. Stat. Phys. 89 (1997) 403–409.
[25] A.L. Garcia, W. Wagner, Some new properties of the kinetic equation for the consistent Boltzmann algorithm, Transport Theor. Stat. 31 (2002) 579–594.
[26] P.P.J.M. Schram, Kinetic Theory of Gas and Plasmas, Kluwer Academic Publishers, Dordrecht, 1991.
[27] J.M. Montanero, A. Santos, Monte Carlo simulation method for the Enskog equation, Phys. Rev. E 54 (1996) 438–444.
[28] J.M. Montanero, A. Santos, Simulation of the Enskog equation a la Bird, Phys. Fluids 9 (1997) 2057–2060.
[29] A. Frezzotti, A particle scheme for the numerical solution of the Enskog equation, Phys. Fluids 9 (1997) 1329–1335.
[30] M. Wang, Z.X. Li, An Enskog based Monte Carlo method for high Knudsen number non-ideal gas flows, Comput. Fluids 36 (8) (2007) 1291–1297.
[31] H.A. Hassan, D.B. Hash, A generalized hard-sphere model for Monte Carlo simulation, Phys. Fluids A 5 (1993) 738–744.
[32] J. Fan, A generalized soft-sphere model for Monte Carlo simulation, Phys. Fluids 14 (2002) 4399–4405.
[33] M. R Wang, Z.X. Li, Numerical simulations on performance of MEMS-based nozzles at moderate or low temperatures, Microfludics Nanofludics 1 (1) (2004) 62–70.
[34] J.G. Aston, J.J. Fritz, Thermodynamics and Statistical Thermodynamics, John Wiley & Sons, New York, 1959.